

1 Silicon isotopic systematics of deep-sea sponge grounds in the North Atlantic

2 Katharine R. Hendry¹, Lucie Cassarino¹, Stephanie L. Bates¹, Timothy Culwick¹, Molly Frost¹, Claire
3 Goodwin², Kerry L. Howell³

4 ¹ School of Earth Sciences, University of Bristol, Wills Memorial Building, Queen's Road, Bristol BS3
5 1NH, United Kingdom

6 ² Huntsman Marine Science Centre, 1 Lower Campus Rd, Saint Andrews, New Brunswick, E5B 3A3,
7 Canada

8 ³ School of Biological and Marine Sciences, Plymouth University, Drake Circus, Plymouth, PL4 8AA,
9 United Kingdom

10

11 Keywords: Porifera, isotopes, silicic acid, geochemical archives

12

13 Abstract

14 Reconstruction of silica cycling in the oceans is key to a thorough understanding of past
15 climates because of the inherent links between the biogeochemistry of silicifiers and sequestration
16 of organic carbon. Diatoms are one of the most important phytoplankton groups in determining
17 export production from surface waters, and rely largely on upwelling deeper waters as a source of
18 dissolved silicon, an essential nutrient for their growth. Quantification of changes in deep water
19 dissolved silicon concentrations in the past allows a more robust understanding of changes in
20 surface nutrient supply and whole-ocean silicon cycling, but cannot be achieved using surface-
21 derived geochemical archives. In the last few years, there has been increasing focus on the use of
22 geochemical archives in siliceous skeletal elements, or spicules, from seafloor-dwelling sponges to
23 fill this gap. The stable silicon isotopic composition of spicules has been shown to be a function of
24 ambient dissolved silicon, providing a potential archive for past changes in bottom water nutrients.
25 However, biomineralisation processes impact silicon isotope fractionation and silica formed by
26 atypical processes (derived from carnivorous sponges, hypersilicified spicules, and giant basal
27 spicules) result in anomalous geochemical signatures. Furthermore, there is considerable scatter in
28 the calibration between spicule silicon isotopes and dissolved silicon in seawater, even when the
29 atypical groups have been removed. Here, we explore this variability further, by examining
30 aggregation and assemblage-level differences in isotopic fractionation, using silicon isotopic
31 measurements of specimens from two monospecific sponge groups (*Pheronema carpensteri* and

32 *Vazella pourtalesi*), and one mixed-species population (genus *Geodia*) from the North Atlantic. Our
33 new data reveal that variability within the monospecific aggregations is less than mixed-species
34 assemblage, pointing towards a genetic control in isotopic fractionation. However, there is still
35 variability within the monospecific aggregations, which cannot be explained by macroscale
36 environmental differences: such variability is likely a reflection of the physiological health of the
37 individuals, or highly localised heterogeneities in sponge habitats.

38 Other challenges remain in the interpretation of spicule silicon isotopes as proxies for
39 dissolved silicon changes through time, especially when investigating periods of Earth history that
40 extend back considerably further than the residence time of dissolved silicon in the oceans. Despite
41 all the questions still surrounding the use of sponge silicon isotopes in palaeoceanographic
42 applications, they are still the only known archive of bottom water dissolved silicon. Continued
43 efforts to understanding sponge biomineralisation and to incorporate silicon isotopes into oceanic
44 models will help to improve further the reliability of the archive.

45 **1. Introduction**

46 *1.1. The marine silicon cycle: why study the deep?*

47 The marine biological pump plays a key role in the carbon cycle, through the uptake of
48 carbon from the atmosphere (CO₂) during algal growth and subsequent sequestration of carbon via
49 the burial of organic matter at depth. The majority of marine production, occurring away from direct
50 inputs of nutrients, is supported by upwelled nutrients supplied through the remineralisation of
51 sinking particles or release from seafloor sediments. Diatoms, a photosynthetic algae, are
52 responsible for a significant proportion, up to 40%, of primary production in the oceans (Tréguer et
53 al., 2018). Their absolute requirement for dissolved silicon (DSi, in the form of silicic acid) to build
54 their silica tests or frustules, means that there is a fundamental link between both the cycling of
55 silicon and carbon within the climate system (first described by DeMaster, 1979; more recently
56 reviewed by Tréguer and De la Rocha, 2013). The robust quantification of DSi within deep and
57 upwelling waters through time is essential if we are to understand the growth of diatoms in the
58 surface of the world's oceans, the drawdown of CO₂, and the burial of organic matter (Hendry and
59 Brzezinski, 2014).

60 In addition to diatoms, there are a wide range of other organisms that precipitate DSi from
61 seawater (silicifiers) including bacteria (Baines et al., 2012), other single-celled eukaryotes (e.g.
62 radiolarians, silicoflagellates, choanoflagellates, some haptophytes, plants, and animals (Hendry et
63 al., 2018; Marron et al., 2016)). Sponges are the most significant group of animals that contribute to

64 the marine silicon cycle, because the phylum contains a number of silicifying groups requiring a large
65 supply of DSi to form their skeletal elements, or spicules. Unlike diatoms, sponges are seafloor-
66 dwelling and obtain the required DSi from bottom waters rather than surface waters. Given the
67 cosmopolitan distribution of sponges and the high preservation potential of siliceous spicules
68 (Maldonado et al., 2011; Schrader, 1972), they may possibly form a substantial standing stock of
69 sedimentary biogenic silica (BSi) in some continental shelf regions (Maldonado et al., 2011), but will
70 also provide an important archive of the geochemical signature of bottom waters. The occurrence of
71 sponge spicules, over the entire Phanerozoic (Antcliffe et al., 2014), has led to their investigation as
72 potentially useful archives of past oceanic change, especially for deep-water DSi through time (De La
73 Rocha, 2003).

74 *1.2. Aims of this review*

75 Given the reliance of diatoms, and other surface-dwelling silicifiers, on upwelling supplies of
76 DSi, there is substantial motivation to understand the geochemical signatures recorded in marine
77 sponges, which could act as palaeoceanographic proxies for past changes in marine silicon cycling.
78 The silicon isotope composition (denoted by $\delta^{30}\text{Si}$) of sponges has shown promise as a proxy for past
79 bottom-water DSi, due to the discovery of a statistically significant correlation between sponge
80 silicon isotopic fractionation and ambient DSi (Hendry et al., 2010; Wille et al., 2010). Here, we
81 review the developments in the understanding of silicon isotope fractionation by sponges during
82 spicule formation, including recent studies highlighting anomalous fractionation during some forms
83 of biomineralisation, and their use in palaeoceanographic studies. We will present new $\delta^{30}\text{Si}$ data
84 investigating populations of sponges from North Atlantic sponge grounds, specifically to assess
85 variation in isotopic composition of individuals from mono-specific aggregations and multi-specific
86 assemblages. Variation between these individuals, which have grown under almost identical
87 environmental conditions, can be used to address physiological impacts (e.g. growth rate, food
88 supply, health) on spicule $\delta^{30}\text{Si}$ compositions, and the potential impact of these biogeochemically
89 important grounds on the use of spicules as geochemical archives. Finally, we will use our new data
90 together with published data in the literature to re-evaluate the $\delta^{30}\text{Si}$ -DSi calibration.

91 **2. Sponges as geochemical archives**

92 *2.1. Sponge silicification: the role of enzymatic processes*

93 Sponges are predominantly filter-feeding benthic animals (Phylum Porifera), with an
94 ancestral body plan comprising a gelatinous mesohyl surrounded by two layers of cells. Water is
95 circulated throughout the body via a series of pores in an aquiferous “canal” system, aided by

96 flagellated choanocyte cells. Other cells have specialised and changeable functions, including
97 reproduction, digestion, collagen production, and spicule formation. Spicules are produced from
98 carbonate, proteins, or BSi in the case of Classes Demospongea, Homoscleromorpha, and
99 Hexactinellida. These siliceous structures are highly diverse in their morphology, and are produced in
100 – at least initially – and assembled in specialised sclerocytes before being exported out of the cell,
101 where silicification is completed. Spicules can be separated, joined at nodes, or fused by secondary
102 silica (Hooper and Van Soest, 2002). Despite being of great interest for biomaterials research (Jo et
103 al., 2016), the biochemical pathways involved in spicule silicification are not fully understood.
104 Silicification in sponges is generally considered to be controlled by two enzymes: silicatein, which
105 promotes polycondensation reactions, and silicase, which dissolves silica (Müller et al., 2013; Müller
106 et al., 2007; Schroeder et al., 2003). Most spicules are formed in layers around a central filament of
107 silicatein (Shimizu et al., 1998), resulting in a central “axial” canal structure in the final form.
108 However, molecular data suggest the enzymes involved in silicification may have evolved
109 independently multiple times, occurring in individuals that do not express the silicatein gene, and
110 may have been lost as a trait in some non-silicifying lineages (Riesgo et al., 2015).

111 Regardless of the specific biochemical pathway, DSi is a requirement for silicification, and
112 DSi availability is an important factor in determining the distribution of sponges in the oceans
113 (Howell et al., 2016). The uptake of DSi is regulated by availability, and growth experiments in
114 laboratory-cultured sponges reveal that there is a Michaelis-Menten relationship between uptake
115 and DSi concentration, indicative of enzymatic control (López-Acosta et al., 2018; López-Acosta et
116 al., 2016; Maldonado et al., 2011; Reincke and Barthel, 1997). For some shallow-water species, such
117 experiments have shown that significant uptake only occurs when DSi concentrations far exceed
118 natural ambient conditions, which has led to the proposition that these sponges suffer chronic
119 silicon limitation (Maldonado et al., 2012). The measured kinetic parameters vary both between and
120 within species, indicating both an evolutionary control on the nature and functioning of these
121 enzymes, in addition to an influence of physiological factors such as food availability and health on
122 DSi uptake (López-Acosta et al., 2016).

123 *2.2. Silicon isotopes in sponges*

124 Sponge biogenic silica is relatively pure, with a general formula $\text{SiO}_2 \cdot n\text{H}_2\text{O}$, with a greater and
125 more variable degree of hydration relative to diatom silica. Given the trace abundance of
126 incorporated metals, the majority of proxy calibration studies have focused on the use of silicon
127 isotopes as geochemical tracers, although there have been some studies into the use of some trace
128 elements and their isotopes e.g. zinc and germanium (Guillermic et al., 2017; Hendry and Andersen,

129 2013). Oxygen isotopes in spicules have been the focus of a small number of studies, and appear to
 130 exhibit a high degree of variability, which is not yet mechanistically understood (reviewed in Hendry
 131 et al., 2015).

132 Silicon has three stable isotopes (^{28}Si , ^{29}Si and ^{30}Si), and fractionation of these isotopes
 133 occurs in natural systems as a result of physical, chemical or biochemical reactions. The silicon
 134 isotopic composition ($\delta^{30}\text{Si}$, Equ. 1) of spicules, and the associated fractionation of silicon with
 135 respect to seawater (denoted by $\Delta^{30}\text{Si}$, Equ. 2), is highly variable (Hendry et al., 2010; Wille et al.,
 136 2010) and under certain conditions can be greater than fractionation observed for other silicifiers
 137 such as diatoms or radiolarians (Abelmann et al., 2015; Hendry et al., 2014).

$$138 \quad \delta^{30}\text{Si} = \left\{ \left[\frac{\left(\frac{^{30}\text{Si}}{^{28}\text{Si}} \right)_{\text{sample}}}{\left(\frac{^{30}\text{Si}}{^{28}\text{Si}} \right)_{\text{NBS28}}} \right] - 1 \right\} \times 1000 \quad (1)$$

$$139 \quad \Delta^{30}\text{Si} = \delta^{30}\text{Si}_{\text{sponge}} - \delta^{30}\text{Si}_{\text{seawater}} \quad (2)$$

140

141 Although sponge $\delta^{30}\text{Si}$ values were measured for the first time in the 1980s (Douthitt, 1982),
 142 spicule silicon isotopes were first postulated as a potential archive of seawater chemistry decades
 143 later (De La Rocha, 2003). Later studies of modern filter-feeding sponges (both hexactinellid and
 144 demosponges) revealed a statistically significant non-linear relationship between $\delta^{30}\text{Si}$ (and $\Delta^{30}\text{Si}$)
 145 and ambient DSi concentrations in Southern Ocean sponges (Hendry et al., 2010; Hendry et al.,
 146 2011; Wille et al., 2010), and in core-top spicules and living sponges from the Atlantic and Pacific
 147 Oceans (Hendry and Robinson, 2012) (Fig. 1). The same relationship between $\delta^{30}\text{Si}$ and DSi was
 148 found in sponges from the different ocean basins, despite growing in contrasting temperature,
 149 salinity and pH conditions, without any systematic difference between hexactinellid and
 150 demosponges, suggesting that DSi availability is the main driving factor behind $\delta^{30}\text{Si}$ variability in
 151 sponges (Hendry & Robinson, 2012). The $\delta^{30}\text{Si}$ -DSi relationship is thought to derive from the similar
 152 non-linear dependence of sponge growth rate on DSi availability (Hendry and Robinson, 2012; Wille
 153 et al., 2010), where the silicon isotopic fractionation can be expressed following Milligan et al.
 154 (2004), according to Equ. 3.

$$155 \quad \Delta\delta^{30}\text{Si} \approx \varepsilon_f = \varepsilon_{tI} + (\varepsilon_p - \varepsilon_{tE}) \frac{v_E}{v_I} \quad (3)$$

156 where ε_f = the total Si isotopic fractionation factor, ε_{tI} = Si isotopic fractionation due to transport into
 157 the cell, ε_p = Si isotopic fractionation due to polymerisation and ε_{tE} = Si isotopic fractionation due to
 158 transport out of the cell; v_E = rate of Si efflux and v_I = rate of Si influx. This equation can be
 159 rearranged (Equ. 4-5, Wille et al., 2010):

$$160 \quad \varepsilon_f = \varepsilon_{tl} + \Delta\varepsilon_p \left\{ 1 - \frac{\frac{v_{\max p}}{\left(\frac{K_{mp}}{[DSi]}\right)^{+1}}}{\frac{v_{\max l}}{\left(\frac{K_{ml}}{[DSi]}\right)^{+1}}} \right\} \quad (4)$$

$$161 \quad K_{ml} = v_{\max l} \times \frac{K_{mp}}{v_{\max p}} \quad (5)$$

162 where $\Delta\varepsilon_p = (\varepsilon_p - \varepsilon_{tl})$; K_{ml} and K_{mp} are the half saturation constants for DSi incorporation and silica
 163 precipitation respectively, and $v_{\max l}$ and $v_{\max p}$ are the maximum incorporation and precipitation rates
 164 respectively. This relationship was used to reconstruct the general behaviour of silicon isotopic
 165 fractionation by filter-feeding sponges, lending strength to the hypothesis that this fractionation is
 166 driven by enzymatic processes within sclerocytes (Hendry and Robinson, 2012; Wille et al., 2010).

167 More recent work has highlighted that this simple non-linear relationship can breakdown
 168 when distinct biomineralisation processes are active within different groups of sponges. For
 169 example, carnivorous sponges (Vacelet, 2006) that are currently classed in the family Cladorhizidae
 170 (Order Poecilosclerida) are thought to have different isotopic systematics compared to the more
 171 ancestral body forms. Cladorhizids secondarily evolved the carnivorous habit as an adaptation to
 172 low-nutrient conditions (Vacelet and Duport, 2004), and have abandoned the ancestral body
 173 organisation (i.e. the aquiferous “canal” system) and instead possess specialised feeding apparatus
 174 and a closed “circulation” system. One specimen in the genus *Asbestopluma* from the Southern
 175 Ocean (Fig. 2A) (Goodwin et al., 2016) was found to be isotopically heavier than expected for given
 176 ambient DSi concentration, likely a result of different biomineralising mechanisms and internal
 177 fractionation (Hendry et al., 2015). Specialised spicules, desmas, which reinforce the skeleton,
 178 appear to be particularly linked with anomalous $\delta^{30}\text{Si}$. These desmas lack a central canal, and are
 179 thought to grow via a mechanism different to filter-feeding relatives, in agreement with the
 180 hypothesis that some biochemical pathways for sponge biosilicification evolved independently
 181 between different lineages (Maldonado and Riesgo, 2007).

182 Other unusual forms of biosilicification have been shown to exhibit $\delta^{30}\text{Si}$ values that deviate
 183 significantly from the original calibration (Fig. 1). The giant spicules of the Indian and Western Pacific
 184 hexactinellid sponge, *Monorhaphis chuni* (Hooper and Van Soest, 2002), are an extreme example of
 185 biosilicification, with large, basal spicules observed to grow over a metre in length (Jochum et al.,
 186 2017; Wang et al., 2009) (Fig. 2B). Laser analysis of *M. chuni* spicule silicon isotope composition
 187 reveals significantly heavy signatures relative to other sponges, again most likely a result of a
 188 fundamentally different silicification process. Despite this offset, there does appear to be a
 189 significant trend between $\delta^{30}\text{Si}$ and DSi concentrations in *M. chuni*, indicating that they have
 190 potential as a complementary palaeoceanographic archive (Jochum et al., 2017). Analyses of mixed-

191 sponge assemblages from seamounts within the Equatorial Atlantic revealed that heavily fused
192 hexactinellid spicules, exhibiting a “dictyonal-type” framework (Fig. 2C), are isotopically lighter than
193 expected. The sponge specimens in the study were graded according to degree of secondary silica
194 fusion: the more secondary silica deposited, the greater the isotopic anomaly (Cassarino et al.,
195 2018). These results indicate that, again, there is a different process involved in producing secondary
196 silica “cement” that fuses primary spicules within hexactinellids.

197 To date, studies have identified anomalous silicon isotope fractionation behaviour in
198 sponges relating to fundamentally different biosilicification mechanisms. However, filter-feeding,
199 non-fused sponges also exhibit variation, as shown by the scatter in the original $\delta^{30}\text{Si}$ -DSi calibration
200 (Fig. 1). Whilst localised changes in environmental parameters (notably DSi) could be responsible for
201 some of this scatter, there has not been a full investigation of how physiological factors, such as
202 growth rate, health and food supply, could impact silicon isotopic fractionation.

203 *2.3. Palaeoclimate applications*

204 Despite the uncertainties in understanding biomineralisation and silicon isotopic
205 fractionation in sponges, there have already been several studies to utilise the sponge silicon isotope
206 proxy for deep-water formation. There are a number of caveats to consider when applying sponge
207 $\delta^{30}\text{Si}$ to the geological record, including the observed variability in fractionation associated with
208 different biosilicification mechanisms. However, this concern can – to a large part – be assuaged
209 through avoiding potentially anomalous spicules, such as desmas (Hendry et al., 2015), or framework
210 structures (Cassarino et al., 2018). Some palaeoceanographic studies have circumvented potential
211 issues by picking only one form of spicule from marine sediments for archive generation (Fontorbe
212 et al., 2016).

213 Other caveats in the use of the sponge $\delta^{30}\text{Si}$ proxy are more challenging to circumvent. Most
214 critically, the residence time of silicon in the oceans is estimated as 10-15 ka (Georg et al., 2009),
215 with the consequence that whole-ocean silicon concentration – and isotopic budgets – could shift on
216 glacial-interglacial timescales. Changes in terrestrial weathering relating to the growth and retreat of
217 ice sheets are likely to be one of the most important causes of regional or global seawater silicon
218 isotope composition ($\delta^{30}\text{DSi}$) relevant to the majority of silica $\delta^{30}\text{Si}$ records to date (Frings et al.,
219 2016; Hawkings et al., 2018; Opfergelt et al., 2013). Changes in regional DSi utilisation, and so
220 isotopic distillation, by diatoms over abrupt climatic events also need to be taken into consideration
221 (e.g. Hendry et al., 2012). Shifts in whole-ocean silicon isotope systematics could be even more
222 substantial (and challenging to constrain) over long-term geological timescales, in response to
223 changes in continental silicate weathering due to mountain building or macroevolutionary changes.

224 Whilst there is no available proxy for secular changes in silicon budgets, ocean modelling can be
225 used to constrain potential changes through time (De La Rocha and Bickle, 2005).

226 Most palaeoclimate studies have focussed on the Late Quaternary, especially the last
227 deglaciation and into the Holocene, during periods of time that are less likely to have witnessed
228 large shifts in whole-ocean silicon cycling budgets. The first continuous sponge $\delta^{30}\text{Si}$ records
229 investigated impact of whole-ocean circulation shifts of the silicon cycle between glacial and
230 interglacial states by comparing spicule composition at the Last Glacial Maximum (LGM,
231 approximately 20 ka) and the modern. A shift in sedimentary sponge $\delta^{30}\text{Si}$ records between the LGM
232 and today indicate increased deep water DSi concentrations in some sectors of the Southern Ocean,
233 especially the Pacific Sector, consistent with changes in diatom productivity and opal export (Chase
234 et al., 2003; Ellwood et al., 2010; Hendry et al., 2010). Higher resolution spicule archives are
235 beginning to reveal that changes in intermediate and mode water DSi concentrations are also basin-
236 specific. In the Pacific, spicule records suggest that DSi concentrations in intermediate and mode
237 waters were higher throughout the LGM and into the deglaciation, only declining at the beginning of
238 the Holocene, potentially as a result of DSi-enriched deep-water upwelling (Rousseau et al., 2016). In
239 contrast, Atlantic Ocean sedimentary spicule $\delta^{30}\text{Si}$ signatures only record lighter signatures during
240 the abrupt climate events of the deglaciation (Heinrich Event 1 and the Younger Dryas), indicative of
241 enhanced bottom-water DSi concentrations in the mid-depth Atlantic as a result of the millennial-
242 scale reorganisation of ocean circulation (Hendry et al., 2016; Hendry et al., 2014; Hendry et al.,
243 2012).

244 These new Late Quaternary sponge archives have added substantially to the debate over the
245 extent of DSi supply, or “leakage” from the Southern Ocean to the low latitudes on glacial-
246 interglacial timescales, and the subsequent impact on atmospheric pCO_2 . The “silica hypothesis”
247 posited that diatom productivity was promoted by an increase in DSi supplied from dust dissolution
248 during colder glacials (Harrison, 2000). A similar theory, the Silicic Acid Leakage Hypothesis (SALH),
249 was proposed, suggesting that the addition of iron via enhanced dust deposition in the Southern
250 Ocean impacted diatom physiology and macronutrient uptake ratios, resulting in a lower Si:N
251 utilisation ratio and a relative increase in mode or intermediate water DSi (Brzezinski et al., 2002).
252 Low-latitude waters would then receive a relatively high Si:N supply, promoting diatoms relative to
253 other phytoplankton, contributing to pCO_2 drawdown via alkalinity changes (Matsumoto and
254 Sarmiento, 2008). However, the new sponge archives, in combination with other novel proxy data,
255 suggest an alternative theory, termed the Silicic Acid Ventilation Hypothesis (SAVH), which proposes
256 that changes in ventilation of deep waters in the Southern Ocean during these periods enhanced the

257 relative DSi concentration of waters leaking into the lower latitudes, rather than surface productivity
258 (Hendry and Brzezinski, 2014).

259 Spicule records have also been combined with other geochemical archives, including $\delta^{30}\text{Si}$
260 records from diatoms and other silicifiers, to capture the whole silicon cycle (Abelmann et al., 2015;
261 Hendry et al., 2014; Horn et al., 2011). For example, Horn et al. (2011) combined diatom $\delta^{30}\text{Si}$ and
262 nitrogen isotope ($\delta^{15}\text{N}$) archives with sponge $\delta^{30}\text{Si}$ records from the Southern Ocean (Hendry et al.,
263 2010) to show that DSi utilisation was high during the deglacial at the same time as deep-water DSi
264 concentrations and supply rates were enhanced, suggesting a strong biological pump and CO_2
265 drawdown. Spicule archives can also be combined with diatom and sponge germanium-to-silicon
266 ratios (Ge/Si) to take whole-ocean changes in silicon inventories into consideration (Ellwood et al.,
267 2010). This approach is based on the observation that diatoms record Ge/Si of surface seawater,
268 whereas sponge Ge/Si is highly fractionated and related to their ambient DSi concentrations
269 (Ellwood et al., 2006). Any common change between Ge/Si in the two siliceous groups can be used
270 to isolate whole-ocean changes in seawater Ge/Si. Whilst a change in this ratio could signify a
271 change in either element, or both, modelling can be used to extract any signal of whole-ocean
272 changes in silicon budgets from sponge $\delta^{30}\text{Si}$ archives (Ellwood et al., 2010).

273 The giant spicules of *M. chuni* have also been used to construct palaeoceanographic records,
274 using laser ablation to derive $\delta^{30}\text{Si}$ profiles across latitudinal sections of individual spicules, which are
275 thought to be able to live up to 18 ka (Jochum et al., 2017). The offset from the original calibration
276 profile (Fig. 1) can be taken into consideration using a novel species-specific calibration (Jochum et
277 al., 2017). However, whilst *M. chuni* represents a novel and independent proxy, there are still
278 challenges in deriving independent age models with which to link the observed geochemical signals
279 with climatic events.

280 Over longer, geological timescales, the influences of whole-ocean changes become more
281 significant, and robust interpretation of sponge $\delta^{30}\text{Si}$ archives requires modelling to assess potential
282 influences of seawater DSi isotopic shifts. Cenozoic sponge $\delta^{30}\text{Si}$ records have been constructed, and
283 combined with isotopic evidence from other silicifiers to track changes in silicon cycling as far back
284 as the Palaeogene (Egan et al., 2013; Fontorbe et al., 2016; Fontorbe et al., 2017). These records
285 highlight that a “modern-like” marine silicon cycle was established early in the Cenozoic, with a
286 proto-Southern Ocean silicon cycle characterised by upwelling of DSi-rich deep-waters and strong
287 utilisation by diatoms (Egan et al., 2013), and an Atlantic-Pacific gradient in DSi concentrations
288 (Fontorbe et al., 2017), from Eocene-Oligocene boundary. Isotopically heavy spicules and
289 radiolarians from Atlantic sediments indicate low DSi concentrations in low-latitude waters well

290 before the Eocene diversification of diatoms (Fontorbe et al., 2016). This early drawdown of DSi has
291 been used, in combination with molecular studies (Marron et al., 2016), as evidence that other
292 pelagic silicifiers and early diatoms may have had more impact on the marine silicon cycle than
293 previously thought (Conley et al., 2017).

294 **3. Sponge grounds in the North Atlantic: silicon isotopes at the population level**

295 *3.1. Sponge grounds of the North Atlantic*

296 Sponge grounds, comprising dense aggregations or assemblages of sponges, are found
297 throughout the North Atlantic. These environments are important for biogeochemical cycling,
298 biodiversity, and natural products (Cathalot et al., 2015; Hogg et al., 2010; Kenchington et al., 2013;
299 Maldonado et al., 2017), and are highly vulnerable to anthropogenic damage and oceanic change
300 (Beazley et al., 2018; Howell et al., 2016). Given that these sponge grounds are well-characterised,
301 they are also ideal testing grounds for population-level isotopic variation.

302 We have selected three different locations to test population level $\delta^{30}\text{Si}$ variation (Fig. 3,
303 Table 1):

- 304 i) Porcupine Seabight: *Pheronema carpenleri* (Order Amphidiscosida, Family
305 Pheronematidae) monospecific ground from the Northeast Atlantic (Howell et al., 2016;
306 Rice et al., 1990);
- 307 ii) Nova Scotia: *Vazella pourtalesi* or 'Russian Hat' sponge (Order Lyssacinosida, Family
308 Rosselidae) monospecific ground, from Emerald Basin (2016) and Sambro Bank Closure
309 (2017) of the Northwest Atlantic shelf (Beazley et al., 2018);
- 310 iii) Labrador Sea: *Geodia* spp. (Order Tetractinellida, Family Geodiidae) multi-specific
311 assemblages from the Boreal-Arctic astrophorid grounds/"boreal ostur" of Orphan Knoll
312 and shelf-environments of Southwest Greenland within the Labrador Sea (Beazley et al.,
313 2013; Howell et al., 2016; Knudby et al., 2013; Murillo et al., 2012).

314 *3.2. Conductivity, temperature, depth (CTD) profiles and water sampling*

315 *3.2.1. Porcupine Seabight*

316 Water data for the Porcupine Seabight were obtained from the electronic World Ocean
317 Circulation Experiment database eWOCE (<http://www.ewoce.org/>).

318 *3.2.2. Nova Scotia*

319 During the expedition to the Emerald Basin in 2016, a continuous, full-depth profile of temperature,
320 salinity, oxygen, and fluorescence, to within 10 m of bottom was made using an SBE 19plus CTD
321 close to the site of sponge collection. A 10-L sampling bottle was closed to collect water for
322 biological and chemical analyses 10 m off the seabed (Fig. A1). During the Sambro Bank expedition in
323 2017, a continuous, full-depth profile of temperature and salinity was made using an SBE 25 CTD
324 close to the site of sponge collection (Fig. A2). Nutrient data were obtained from archived data
325 collected as part of the Atlantic Zone Monitoring Program (AZMP).

326 3.2.3. Labrador Sea and coastal Greenland

327 Samples were collected from Orphan Knoll and Southwest Greenland during RRS Discovery
328 cruise DY081 in July/August 2017. All CTD casts (Fig. A3, A4) were undertaken during DY081 using a
329 SBE 9plus underwater unit with an array of sensors, with 10L Niskin water samplers used to collect
330 water for geochemical analysis (Hendry, 2017).

331 3.3. Sponge collection

332 *Pheronema carpensteri* (Hexactinellida) were sampled using the Irish national remotely
333 operated vehicle (ROV), *Holland I*, from Porcupine Seabight (North East Atlantic) aboard the R/V
334 Celtic Explorer, EUROFLEETS2 cruise CE15011 (Howell et al., 2015). The manipulator arm on the ROV
335 was used to either grab sponges at the base via the anchor spicules, or to scoop sponges up using a
336 metal mesh scoop. Sponges were then placed into bio-boxes mounted on the ROV.

337 *Vazella pourtalesi* (Hexactinellida) were collected using either a box corer or by ROV, *ROPOS*,
338 from the Emerald Basin (North West Atlantic) aboard the R/V Hudson (cruise HUD16019) in July and
339 August 2016 (Kenchington et al., 2016), and using *ROPOS* from the Sambro Bank on the CCGS
340 Martha L. Black (cruise MLB2017001) in July 2017 (Beazley et al., 2017). Hexactinellid morphometrics
341 were recorded when possible (body width and height).

342 *Geodia* sp. (Demosponge) were collected from Orphan Knoll (Labrador Sea) by the ROV, *Isis*,
343 aboard the RRS Discovery in July 2017 (cruise DY081; Hendry et al., 2017). Sponges were collected
344 either using the manipulator arms, or using a suction system.

345 In each case, upon recovery of the ROV to the surface, sponge samples were transferred to
346 buckets and taken into a wet lab for processing. In the wet lab each sponge sample was labelled,
347 measured and photographed. A sub-sample of each sponge was air-dried, before being placed in
348 individual plastic bags or boxes for transportation.

349 3.4. Sample preparation and analysis

350 3.4.1. *Sponge analyses*

351 Small subsamples were cleaned chemically for organic matter by soaking at room
352 temperature for 24 hours in 30% hydrogen peroxide (reagent grade H₂O₂) and then heating for three
353 hours at 80°C in fresh 30% H₂O₂. The samples were then rinsed in 18 MΩ.cm Milli-Q, heated for
354 three more hours at 80°C in fresh 30% H₂O₂, and rinsed again. Lastly, the samples were rinsed in
355 concentrated nitric acid (in-house distilled HNO₃) a total of two times, rinsed between each stage
356 with Milli-Q water. Approximately 1 mg of cleaned spicules (Fig. 4) were then physically separated by
357 hand from any lithogenic particles, weighed into clean Teflon, and dried down in concentrated HNO₃
358 (in-house distilled) at 120°C. The spicules were then dissolved over three days in 0.4M sodium
359 hydroxide (Analar) at 100°C, before being acidified with 8N HNO₃ (in-house distilled), diluted with
360 Milli-Q and purified using cation exchange resin (Bio-Rad AG50W X12, 200-400 mesh in H⁺ form)
361 following published protocols (Georg et al., 2006; Hendry and Robinson, 2012).

362 The purified solutions were spiked with a magnesium solution and analysed for ²⁸Si, ²⁹Si, and
363 ³⁰Si using a Multi-Collector Inductively Coupled Plasma Mass Spectrometer in medium resolution
364 mode. Sample signals were blank-corrected offline, and mass-bias corrected using magnesium
365 isotope ratios (²⁴Mg, ²⁵Mg, and ²⁶Mg) before being normalised to NBS28 (RM8546) following
366 published methods to calculate both δ²⁹Si and δ³⁰Si values (Hendry et al., 2015). A three-isotope plot
367 shows that δ²⁹Si and δ³⁰Si values for samples and standards fall on a mass-dependent linear curve,
368 with a gradient of 0.51 (Fig. A5). Long-term reproducibility was assessed by repeat measurements of
369 reference standards Diatomite and LMG08, yielding δ³⁰Si of +1.24 ± 0.03‰ and -3.47 ± 0.05‰
370 respectively (2SE, n = 14 and 19 respectively), which fall within error of published values (Hendry et
371 al., 2011; Reynolds et al., 2007). Internal errors, fully propagated from blocks of 20 measurements
372 including blank and mass-bias corrections, were typically 0.05‰ for δ²⁹Si and 0.10‰ for δ³⁰Si.
373 Repeat measurements of δ²⁹Si and δ³⁰Si (e.g. *Vazella* 5-022 from MLB2017001) agreed within ±0.04
374 and ±0.03‰ respectively.

375 3.4.2. *Seawater DSi analyses*

376 Samples for inorganic nutrients were all analysed by comparable methods either at the
377 Bedford Institute of Oceanography (BIO) or in the Plymouth Marine Laboratory (PML) using the
378 latest GO-SHIP protocols (Hydes et al., 2010). The analysis was carried out using a SEAL analytical
379 AAll segmented flow colorimetric auto-analyser using classical analytical techniques for nitrate,
380 nitrite, DSi and phosphate, as described in Woodward and Rees (2001). Seawater nutrient reference
381 materials (KANSO Ltd. Japan), or cross-checked in-house standards, were analysed to check analyser
382 performance and to guarantee the quality control of the final reported data. The typical

383 uncertainties of the analytical results were between 2-3%, and the limits of detection were 0.02 μM
384 for nitrate and phosphate, 0.01 μM for nitrite, and DSi did not ever approach the limits of detection.

385 Water DSi silicon isotope ($\delta^{30}\text{DSi}$) analysis methods are fully described in Cassarino et al.,
386 2018. Briefly, silicon was pre-concentrated twice by the additional of sodium hydroxide (1.2% v/v 1M
387 NaOH, followed by 1% v/v 1M NaOH 24 hours later) to precipitate magnesium hydroxide. The
388 precipitate is rinsed with dilute sodium hydroxide (0.001M NaOH) before redissolution in 8M
389 distilled HNO_3 , dilution in 18 M Ω .cm Milli-Q water, and chemical purification using cation exchange
390 resin as outlined above. Mass spectrometric analysis was carried out as for the sponge samples, with
391 the addition of 0.05M HCl and 0.003M H_2SO_4 to standards and samples prior to analysis to account
392 for any potential matrix effects (Hughes et al., 2011). The ALOHA “300” and “1000” seawater
393 standards were measured alongside the seawater samples to assess analytical accuracy and
394 precision, and yielded values within error of published data ($\delta^{30}\text{Si} = +1.10 \pm 0.15 \text{‰}$ and $+1.43 \pm 0.19$
395 ‰ (2SD internal precision), respectively) (Cassarino et al., 2018; Grasse et al., 2017).

396 3.4.3. *Sponge identification*

397 Sponges from the genus *Geodia* collected during DY081 were identified to species level after
398 collection. To isolate the spicules, sponge tissue was digested in bleach (15% Sodium Hypochlorite).
399 Spicules were then washed twice with water and once in 95% ethanol, allowing the spicules to settle
400 out of the washing solution for ~45 minutes between each change. A few drops of the final ethanol
401 solution were placed on a slide and then this was placed on a heat plate, evaporating the alcohol
402 and leaving the spicules behind. The spicules were mounted in Canada balsam covered with a glass
403 coverslip. A thick tissue section ($\approx 0.2\text{mm}$) was cut using a scalpel and also mounted using Canada
404 balsam. Spicule measurements were made using an Olympus BX43 microscope, with thirty spicules
405 measured per spicule type. Digital photos were taken using the combination of the Olympus BX43
406 microscope with a SC50 camera and are available upon request.

407 3.5. *Sponge ground results: insight into population variance*

408 The new $\delta^{30}\text{Si}$ sponge and seawater $\delta^{30}\text{DSi}$ data are shown in Table A1. The $\delta^{30}\text{Si}$ values for
409 the hexactinellid specimens range from -1.24 to -2.49‰ ; the *Geodia* specimens ranged from -1.08
410 to -2.37‰ .

411 3.5.1. *Monospecific aggregations*

412 The *P. carpenteri* aggregation specimens show a mean $\delta^{30}\text{Si}$ value of -2.07‰ and a variance 0.04‰
413 ($n = 29$; Fig. 5). There is no significant correlation between $\delta^{30}\text{Si}$ and calculated body volume

414 (correlation coefficient = 0.238; $p > 0.05$; Fig. A6), assuming an ellipsoid form. There is also no
415 significant correlation between temperature or salinity and spicule $\delta^{30}\text{Si}$ ($p > 0.05$).

416 Compared to the *P. carpenteri* samples, the specimens from the *V. pourtalesi* aggregations show
417 higher mean $\delta^{30}\text{Si}$ values of -1.59‰ (variance of 0.03‰) and -1.65‰ (variance of 0.02‰) for the
418 Emerald Basin and Sambro Basin specimens respectively. There is no significant difference between
419 either the means (note the low power of this statistical test) or the medians of the two aggregations
420 of *V. pourtalesi* (one-tailed t-test, $p = 0.198$, power = 0.210; rank sum test, $p = 0.603$). The overall
421 variance of the *V. pourtalesi* specimens was 0.02‰ ($n = 24$). There is a significant correlation with
422 body volume (correlation coefficient = 0.758; $p < 0.01$, $n = 12$; Fig. A6), assuming a cylindrical body
423 form. Note not all of the specimens have morphometric data available, so the statistical analysis in
424 this case was carried out on a small subset of specimens, and the correlation is largely driven by one
425 outlier (Fig. A6). Both hexactinellid populations passed a Shapiro-Wilk normality test (Table 2; Fig.
426 5B).

427 Silicon isotope fractionation was calculated using Equation 2 (Table A1), using the measured
428 isotopic composition of the sponge spicules and seawater samples (Fig. 7A). The closest located
429 seawater sample was used for each specimen (or mean values if specimen was located between two
430 Niskin sampling events). Seawater samples were not available for the *P. carpenteri* samples, so a
431 $\delta^{30}\text{DSi}$ value of $+1.5\text{‰}$ was chosen for the ambient composition based on published water column
432 profiles from the Atlantic Ocean (de Souza et al., 2012). The mean $\Delta^{30}\text{Si}$ values for the *V. pourtalesi*
433 and *P. carpenteri* groups were calculated to be -3.21‰ and -3.57‰ respectively. The two groups
434 show equal variance in their population fractionation factors (Brown-Forsythe test passed, $p = 0.438$;
435 both groups have a variance of $\sim 0.04\text{‰}$) but have significantly different means (two-tailed t-test, $p <$
436 0.001 , power 0.998 for $\alpha = 0.05$) with the greater mean fractionation factor observed for the *P.*
437 *carpenteri* population (one-tailed t-test, $p < 0.001$, power 0.999 for $\alpha = 0.05$).

438 3.5.2. Multi-specific assemblages

439 The mean $\delta^{30}\text{Si}$ composition for all the *Geodia* specimens was -1.64‰ , with a variance of
440 0.09‰ ($n = 20$). All *Geodia* specimens, taken as one population, passed a Shapiro-Wilk normality
441 test (Table 2). Although variability between individual is greater for the astrophorids compared to
442 the hexactinellid monospecific aggregations, this group represents a number of different species
443 within the same genus. Dividing the group into species (Fig. 6) shows that some of the variability
444 could be a result of genetic differences. For most of the astrophorids, the variance is more aligned
445 with the hexactinellid populations when separated into species: *G. atlantica*, *G. hentscheli*, *G.*
446 *macandrewii*, and *G. nodostrella* all have closely aligned isotopic compositions despite not having

447 close phylogenetic relationships (Cardenas et al., 2013). However, *G. hentscheli*, *G. parva* and *G.*
448 *phlegraei* are more variable (*G. parva* and *G. phlegraei* groupings both have lighter isotopic
449 specimens, and are closely allied on the molecular phylogeny of the genus). *G. barretti* is significantly
450 heavier than the majority of the other specimens, although the specimen was the only one located
451 in the northern-most collection site off west Greenland.

452 Initial tests indicated that different spicules from an astrophorid from the Southern Ocean
453 have the same $\delta^{30}\text{Si}$ composition within uncertainty ($\delta^{30}\text{Si}$ of $-2.87 \pm 0.21\text{‰}$ and $-2.96 \pm 0.23\text{‰}$ for
454 subsamples of a sterraster-dominated dermal layer and a parenchymal layer respectively) (Hendry et
455 al., 2010). The results here also support a relatively uniform isotopic composition between
456 individuals, at least for most *Geodia* species.

457 Again, the fractionation of silicon isotopes was calculated using Equation 2 (Table A1), using
458 the measured sponge and seawater $\delta^{30}\text{DSi}$ values (Fig. 6). The different *Geodia* species show some
459 variation in $\Delta^{30}\text{Si}$, with mean of -2.94‰ with a variance of 0.08‰ . However, taking the
460 environmental differences in ambient $\delta^{30}\text{DSi}$ between sampling locations, through the calculation of
461 fractionation factors, can only eliminate some of the variation between species. For example, the *G.*
462 *barretti* specimen from the northern sampling site was collected from somewhat isotopically heavier
463 waters than the other specimens (Table A1). The remaining variability must be due to other
464 environmental differences, in addition to physiological differences between the specimens.

465 **4. Discussion**

466 *4.1. New calibration between sponge silicon isotopes and ambient dissolved silicon concentrations*

467 A compilation of all published data reveals the extreme variation in the fractionation of
468 stable silicon isotopes during spicule growth (Fig. 7A and B). There are some significant outliers from
469 the original calibration curve (Fig. 1), which comprise sponges with atypical biosilicification processes
470 including heavily fused hexactinellids (Cassarino et al., 2018); carnivorous sponges (Hendry et al.,
471 2015), and the giant spicules of *M. chuni* (Jochum, 2017). If the atypical silicifiers are removed from
472 the calibration (Fig. 7B), the remaining sponge specimens (largely comprising filter-feeding sponges
473 that produce loose spicules) still show a significant correlation between isotopic fractionation and
474 DSi (Equ. 6):

$$475 \quad \Delta^{30}\text{Si} = -4.6(0.1) + \frac{27.6(1.9)}{(7.4(1.9) \times \text{DSi})} \quad (6)$$

476 (Adjusted $R^2 = 0.46$, $p < 0.001$).

477 *4.2. Potential biological driving mechanisms behind silicon isotopic fractionation in sponges*

478 4.2.1. Differences within species: isotopic variations at the population-level

479 Our new data from the North Atlantic sponge grounds are consistent with the original non-
480 linear DSi- $\delta^{30}\text{Si}$ relationship found previously, especially in comparison to sponges with atypical
481 silicification mechanisms that form clear outliers. However, there is still scatter in the empirical
482 relationship, which can be explored with the results from the monospecific assemblages, and can be
483 used to largely exclude genetic differences as a driving factor in isotopic fractionation. Northwest
484 Atlantic *P. carpenteri* aggregation is isotopically light for the given ambient DSi concentrations and so
485 plots below the main calibration line (Fig. 7A). Given that both the *Pheronema* and *Vazella* genera
486 belong to orders (Amphidiscosida and Lyssacinosa respectively) that are not characterised by
487 fused, dictyonal spicules (Tabachnick et al., 2017), and the specimens analysed here comprised
488 either loose spicules or spicules fused lightly at nodes (Fig. 4), secondary hypersilicification is not a
489 possible mechanism for driving silica isotopic compositions towards lighter values (Cassarino et al.,
490 2018).

491 One possible reason behind this variation within a monospecific aggregation is that there are
492 variations in the growth rate (linked with food supply, or health) between the individuals and, so,
493 differences in the specific values of the uptake kinetics parameters and a variation in isotopic
494 fractionation (Equation 4). However, a lack of relationship between body size and $\delta^{30}\text{Si}$ in the *P.*
495 *carpenteri* samples, and only a statistically weak relationship between the parameters in the *V.*
496 *pourtalesi* specimens, argues against a growth rate effect in this case (Fig. A6).

497 An alternative explanation as to why these sponge ground specimens have more negative
498 $\delta^{30}\text{Si}$ values than expected – or predicted by the biological model shown in Equation 4 – is that the
499 sponges obtain DSi for biomineralising partially from recycled sponge silica, which is available as a
500 result of the close proximity of the densely aggregated individuals. We have constructed a simple
501 model to test this hypothesis, varying the percentage of DSi taken up by the sponge originating from
502 recycled spicules rather than bottom waters, and using isotopic mass balance to calculate the
503 subsequent impact on spicule $\delta^{30}\text{Si}$ values (Table A2). Our model implies that the *P. carpenteri*
504 sponges could be biomineralising from a solution comprising 40-60% recycled silica, with a lower
505 degree of recycling (<40%) occurring in the *V. pourtalesi* aggregations (Fig. 8). A high degree of
506 recycling in *P. carpenteri* sponge grounds is consistent with the observation of thick spicule mats,
507 with aggregations of living and dead sponges commonly found together (Barthel et al., 1996; Bett
508 and Rice, 1992). Variations in the extent of spicule recycling could be responsible for the isotopic
509 fractionation scatter observed in population level in dense sponge grounds.

510 4.2.2. Differences between species in a mixed assemblage

511 The relationship between DSi and $\delta^{30}\text{Si}$ for filter-feeding, non-hypersilicified sponges that are
512 found in mixed assemblages still shows a degree of scatter, even when atypical silicification processes
513 are accounted for and removed from the calibration. Despite growing under almost identical
514 environmental conditions, mixed assemblages of sponges from a particular area exhibit a wide range
515 in $\delta^{30}\text{Si}$, a larger range than for monospecific aggregations (e.g. Cassarino et al., 2018). Part of this
516 variability could be a result of silica recycling (Fig. 8), although this mechanism can only drive the
517 system towards lighter isotopic compositions.

518 Instead, the variation could be a result of a combination of genetic variation and physiology.
519 Our new *Geodia* results show that, generally, a good proportion of the scatter in isotopic composition
520 can be accounted for by species-specific variations in fractionation (Fig. 6). The half saturation
521 constant and maximum incorporation rate for polymerisation varies between species, and potentially
522 even within species as a result of differences in food availability or health (López-Acosta et al., 2018;
523 López-Acosta et al., 2016). We have explored the impact on silicon isotopic fractionation of such
524 differences in uptake parameters using the simple biological model in Equation 4 (Cassarino et al.,
525 2018), and found that a large degree of variability can be explained by differences in kinetics between
526 species (Fig. 9A and B).

527 The majority of the analyses of sponge $\delta^{30}\text{Si}$ variation to date have been carried out in deep
528 water sponges, where environmental variability is relatively low. Shallow water sponges, especially
529 those in the littoral or sublittoral zone, are likely to be subject to extreme environmental changes on
530 a range of timescales (diurnal, seasonal, annual), and so could be expected to show a larger degree
531 of isotopic variability driven by ambient conditions. Any differences in silicon isotope fractionation
532 between species may also be expected to be amplified, depending on factors such as growing season
533 and growth rate. Quantifying the variability in sponge $\Delta^{30}\text{Si}$ in these ecosystems may be particularly
534 challenging, given the requirement to characterise changes in sponge growth and ambient
535 conditions (e.g. seawater $\delta^{30}\text{Si}$ variations) over a range of spatial scales.

536 4.2.3. Differences between higher taxonomic rankings

537 There are fundamental differences in biosilicification between hexactinellids and
538 demosponges, which might be expected to manifest in contrasting isotopic fractionation (Cassarino
539 et al., 2018). Demosponges fuse the concentric silica layers that form around the axial canal,
540 whereas they remain distinct layers in hexactinellids (Aizenberg et al., 2005; Müller et al., 2009;
541 Wang et al., 2011). Furthermore, the organic composition of the silicification proteins in the two
542 groups differ: hexactinellids have higher molecular weight proteins than those isolated from

543 demosponges (Weaver et al., 2003). The interaction between the polymerising silica and these
544 different organic molecules could result in divergent isotopic fractionation (Cassarino et al., 2018).

545 Despite these clear differences in silicification mechanism, there is no clear answer at this
546 stage as to what extent are there differences in isotopic behaviour between hexactinellids and
547 demosponges. A qualitative analysis of the whole dataset (excluding 'lithistids', *Asbestopluma* sp.
548 and *M. chuni*) suggests that the DSi- $\delta^{30}\text{Si}$ relationships are different between hexactinellids and
549 demosponges (Fig. 7B). However, this whole dataset also illustrates that the two groups are
550 separated in DSi "space", with demosponges able to grow under lower DSi concentrations than
551 hexactinellids, such that the difference in isotopic fractionation could be a consequence of distinct
552 habitat preferences. To account for any DSi influence, one approach is to normalise the $\delta^{30}\text{Si}$ data, by
553 calculating a residual for each datapoint relative to the best-fit hyperbolic regression. This method
554 has previously revealed a lack of systematic differences between demosponges and hexactinellids
555 (Cassarino et al., 2018). Alternatively, it is possible to statistically assess the differences in
556 fractionation between the two groups, but only within the DSi range under which both groups are
557 present (10 to 100 μM DSi). Under these constraints, there is no significant difference between the
558 mean $\delta^{30}\text{Si}$, or DSi- $\delta^{30}\text{Si}$ intercepts, of hexactinellids and demosponges once DSi differences are taken
559 into account (ANCOVA, $F=0.045$, $p=0.833$; Fig. A7). This suggests that, despite some fundamental
560 differences in silicification behaviour between hexactinellids and demosponges, there is no
561 significant impact on stable silicon isotopic fractionation, at least for filter-feeding sponges without
562 dictyonal framework skeletons. This suggests that using a mixture of hexactinellid and demosponge
563 spicules, which are often challenging to distinguish within sediments, to measure $\delta^{30}\text{Si}$ variations in
564 marine cores should produce robust and interpretable archives of past oceanic change provided
565 spicules with clearly different morphology (e.g. giant spicules, desmas, heavily fused spicules) are
566 avoided.

567 **Conclusion and outlook**

568 Diatom productivity, and oceanic export production, relies on the upwelling of deep-waters
569 for a supply of dissolved silicon. If we are to quantify future changes in marine carbon cycling, we
570 need to be able to predict future changes in diatom growth and, so, changes in the supply of DSi and
571 other nutrients to the surface through physical and chemical processes. One of the best analogues
572 we have for how the oceans may respond in the future is the geological record: understanding how
573 diatoms have responded to past climate events can inform greatly on potential upcoming change.
574 However, because of the reliance of diatoms on deep-waters, we need an archive of bottom water
575 DSi concentrations if we are to tease apart the relative impacts of changes in physical upwelling as

576 opposed to water mass variability and remineralisation. To date, sponge spicules are the only
577 available archive of deep-water silica, especially spicule $\delta^{30}\text{Si}$ values, which have been shown by a
578 number of studies to have a statistically significant relationship with ambient DSi. There are
579 important caveats, as common to all novel geochemical proxies, which must be taken into
580 consideration for robust interpretation of downcore archives. Atypical biomineralisation processes
581 (hypersilicification, the growth of giant basal spicules, and silica production in carnivorous sponges)
582 have an impact on silicon isotopic compositions. However, these spicule types can largely be
583 disregarded for palaeoceanographic studies as they are morphologically distinct.

584 There are further, more complex challenges surrounding unknown variations in ambient DSi
585 and seawater $\delta^{30}\text{Si}$, either on the small scale in the immediate surroundings of the growing sponge
586 (e.g. silica recycling within dense sponge aggregations or within individuals as shown in this study) or
587 secular changes on large spatial scales and over long periods of time that exceed the residence time
588 of silicon in seawater. However, multi-proxy approaches and modelling efforts will help to
589 understand these challenging caveats. Robust dating methods and age models are also required,
590 which have in spicule $\delta^{30}\text{Si}$ studies – to date – relied entirely on the dating of surrounding material
591 (e.g. by radiocarbon dating or foraminiferal isotope stratigraphy) and do not take into consideration
592 the potential age-differential between sedimentary components. Improvements in radiocarbon
593 dating of sponge organic matter may provide a better handle on how long sponges live, and the
594 absolute ages of spicules within sediments (Fallon et al., 2010). Lastly, and perhaps most
595 fundamentally, we do not have a full understanding of the biochemical pathways that lead to $\delta^{30}\text{Si}$
596 variations between sponges. Our new results show that there is scatter in the spicule DSi- $\delta^{30}\text{Si}$
597 relationship, even between specimens from monospecific aggregations that have grown under the
598 same environmental conditions, indicating that there is more to understand about how the health of
599 individuals can impact biological fractionation of silicon isotopes. A greater understanding of
600 biomineralisation pathways, and how they differ between sponge groups, will aid our mechanistic
601 understanding of how sponges fractionate silicon isotopes.

602 **Acknowledgements**

603 This research was funded by European Research Council project ICY-LAB (ERC-2015-STG
604 grant agreement number 678371), and EU Horizon 2020 project SponGES (H2020-BG-2015-2 grant
605 agreement number 679849). K. L. Howell is funded by the EU Seventh Framework Programme
606 EUROFLEETS2 (FP7/2007-2013 grant agreement number 312762). Thanks to Christopher D. Coath
607 for assistance with mass spectrometry, and Paco Cárdenas for advice on *Geodia* identification. Many
608 thanks to Ellen Kenchington and Lindsay Beazley for collection of *Vazella pourtalesi* sponges and co-

609 located seawater samples, and for supplying details of their previous benthic surveys on Orphan
610 Knoll which assisted with cruise planning. Canadian funding was received from the International
611 Governance Strategy (IGS) fund of the Department of Fisheries and Oceans Canada Project “Marine
612 Biological Diversity Beyond Areas of National Jurisdiction (BBNJ): 3-Tiers of Diversity (Genes-Species-
613 Communities)” to E. K. We also thank Joana Xavier, Manuel Maldonado and Hans Tore Rapp for
614 support through the SponGES project. Many thanks to two anonymous reviewers for their
615 constructive comments.

616 Data availability: An electronic copy of the new data from this study is available at
617 <https://doi.pangaea.de/10.xxxx/PANGAEA.xxxxx>

Location	Species	n	Depth (m)	Temperature (°C)	Salinity	Oxygen ($\mu\text{mol/L}$)	DSi (μM)	NO ₃ (μM)
Porcupine Seabight	<i>Pheronema carpenteri</i>	29	1204 - 1407	6.5 - 7.1	35.2 - 35.4	245 - 255 ^a	11.3 - 11.6 ^a	18.1 - 18.4 ^a
Emerald Basin	<i>Vazella pourtalesi</i>	8	184 - 206	11.0 - 11.1	35.2	121 - 126	16.9 ± 0.5	18.9 ± 0.2
Sambro Basin	<i>Vazella pourtalesi</i>	16	154 - 161	~10	~34.7	200 - 220 ^a	12.0 ± 0.4	17.5 ± 2.6
Orphan Knoll	<i>Geodia</i>	13	1763 - 3463	2.1 - 3.4	34.9	265 - 272	6 - 15	
Coastal Greenland	<i>Geodia</i>	2	846 - 1146	3.9 - 4.5	34.9	280 - 290	9 - 10	

620

	Species	n	W-Statistic	P value	Passed?
	<i>Pheronema carpenteri</i>	29	0.975	0.706	yes
	<i>Vazella pourtalesi</i>	25	0.975	0.796	yes
i)	<i>Emerald Bank</i>	17	0.851	0.097	yes
ii)	<i>Sambro Bank</i>	8	0.956	0.592	yes
	<i>Geodia sp.</i>	20	0.932	0.170	yes

621

622 **Figure captions**

623 Figure 1: Original calibration studies figure (Hendry et al., 2010, Wille et al., 2010; Hendry &
624 Robinson, 2012) of apparent sponge silicon isotope fractionation (denoted by $\Delta^{30}\text{Si}$, Equation 2) and
625 ambient dissolved silicon concentrations (DSi). Symbols highlight the different collection expeditions.
626 Error bars show ranges for DSi in μM , and 2SD for isotopic fractionation.

627 Figure 2: Scanning Electron Microscope images of sponge spicules. A) basal spicules from
628 *Asbestopluma* sp. (Hendry et al., 2015) where des = desmas and ani = anisostrongyes; B) cross-
629 section through spicule of *Monorhaphis chuni* (Jochum et al., 2017); C) fused framework of
630 hexactinellid from the tropical Atlantic (Cassarino et al., 2018).

631 Figure 3: Location of collection sites of the new sponge specimens, from North Atlantic sponge
632 grounds. Black symbols show hexactinellids, yellow symbols show demosponges. Squares show
633 *Vazella pourtalesi* samples from Emerald Basin (solid) and Sambro Basin (hollow); triangles show
634 *Pheronema carpenteri* samples from Porcupine Seabight; stars show *Geodia* (demosponge)
635 specimens from boreal sponge grounds.

636 Figure 4: Scanning Electron Microscope images of *Vazella*, *Pheronema* and *Geodia* specimens, after
637 chemical cleaning and before dissolution. Scale bar shows 100 μm .

638 Figure 5: Silicon isotopic composition ($\delta^{30}\text{Si}$) of sponge-ground forming hexactinellids: A) all
639 datapoints and B) all *Vazella* and *Pheronema* data plotted as histograms. Scale bars show
640 uncertainties based on repeat measurements of sponge standard LMG08 ($\pm 2\text{SD}$).

641 Figure 6: Silicon isotopic composition ($\delta^{30}\text{Si}$) of *Geodia* specimens (black circles). Scale bars show
642 uncertainties based on repeat measurements of sponge standard LMG08 ($\pm 2\text{SD}$). Grey circles show
643 silicon isotopic fractionation ($\Delta^{30}\text{Si}$, see Equation 2).

644 Figure 7: A) Compilation of all Si isotopic fractionation data ($\Delta^{30}\text{Si}$, see Equation 2) for all available
645 sponge spicule studies. Scale bars show fully propagated errors ($\pm 2\text{SD}$). Symbols show different
646 sponge types, where FF = filter-feeding (non-carnivorous) sponges excluding heavily fused
647 hexactinellids and *M. chuni*. (NB: "lithistids" have been removed from the Wille et al., 2010 dataset).
648 B) spicule Si isotope data comparing hexactinellids and demosponges, excluding carnivorous, heavily
649 fused sponges and *M. chuni*.

650 Figure 8: Sponge ground modelling results. Large circles show new data from sponge-ground forming
651 hexactinellids; small grey circles show published data, where FF = filter-feeding (non-carnivorous)
652 sponges excluding heavily fused hexactinellids and *M. chuni*. For model details, see main text.

653 Figure 9: Uptake of silicon by sponges modelled using Michaelis-Menten kinetics. For model details,
654 see main text. A) DSi consumption and B) Si isotopic fractionation (Cassarino et al., 2018). Silicon
655 uptake data from (López-Acosta et al., 2018; López-Acosta et al., 2016; Maldonado et al., 2011;
656 Reincke and Barthel, 1997).

657 **Table captions**

658 Table 1: Specimen sample table, including environmental parameters. ^a From GLODAP dataset.

659 Table 2: Shapriro-Wilk normality test results for specimens from the three sponge grounds.

660

661 **References**

- 662 Abelman, A., Gersonde, R., Knorr, G., Zhang, X., Chaplign, B., Maier, E., Esper, O., Friedrichsen, H.,
663 Lohmann, G. and Meyer, H. (2015) The seasonal sea-ice zone in the glacial Southern Ocean as a
664 carbon sink. *Nature communications* 6.
- 665 Aizenberg, J., Weaver, J.C., Thanawala, M.S., Sundar, V.C., Morse, D.E. and Fratzi, P.J.S. (2005)
666 Skeleton of *Euplectella* sp.: structural hierarchy from the nanoscale to the macroscale. 309, 275-
667 278.
- 668 Antcliffe, J.B., Callow, R.H. and Brasier, M.D. (2014) Giving the early fossil record of sponges a
669 squeeze. *Biological Reviews* 89, 972-1004.
- 670 Baines, S.B., Twining, B.S., Brzezinski, M.A., Krause, J.W., Vogt, S., Assael, D. and McDaniel, H.J.N.G.
671 (2012) Significant silicon accumulation by marine picocyanobacteria. 5, 886.
- 672 Barthel, D., Tendal, O. and Thiel, H.J.M.E. (1996) A Wandering Population of the Hexactinellid
673 Sponge *Pheronema carpenteri* on the Continental Slope off Morocco, Northwest Africa. 17, 603-
674 616.
- 675 Beazley, L.I., Kenchington, E.L., Murillo, F.J. and Sacau, M.d.M. (2013) Deep-sea sponge grounds
676 enhance diversity and abundance of epibenthic megafauna in the Northwest Atlantic. *Journal of*
677 *Marine Science* 70, 1471-1490.
- 678 Beazley, L.I., Pham, C., Murillo, F.J. and Kenchington, E. (2017) Cruise report for the DFO/SponGES
679 CCGS Martha L. Black Oceanographic Mission (MLB2017001), August 31 to September 7, 2017,
680 Canadian Technical Report of Fisheries and Aquatic Sciences 3242. Bedford Institute of
681 Oceanography.
- 682 Beazley, L.I., Wang, Z., Kenchington, E., Yashayaev, I., Rapp, H.T., Xavier, J.R., Murrillo, F.J., Fenton, D.
683 and Fuller, S. (2018) Predicted distribution of the glass sponge *Vazella pourtalesi* on the Scotian Shelf
684 and its persistence in the face of climatic variability. *PLoS One* 13(10), e0205505.
685 <https://doi.org/10.1371/journal.pone.0205505>.
- 686 Bett, B. and Rice, A. (1992) The influence of hexactinellid sponge (*Pheronema carpenteri*) spicules on
687 the patchy distribution of macrobenthos in the porcupine seabight (bathyal ne atlantic). *Ophelia* 36,
688 217-226.
- 689 Brzezinski, M.A., Sigman, D.M., Sarmiento, J.L., Matsumoto, K., Gruber, N., Rau, G.H. and Coale, K.H.
690 (2002) A switch from $\text{Si}(\text{OH})_4$ to NO_3^- depletion in the glacial Southern Ocean. *Geophysical Research*
691 *Letters* 29, 1564.
- 692 Cardenas, P., Rapp, H.T., Klitgaard, A.B., Best, M., Thollesson, M. and Tendal, O.S.J.Z.J.o.t.L.S. (2013)
693 Taxonomy, biogeography and DNA barcodes of *Geodia* species (Porifera, Demospongiae,
694 Tetractinellida) in the Atlantic boreo-arctic region. 169, 251-311.
- 695 Cassarino, L., Coath, C.D., Xavier, J.R. and Hendry, K.R. (2018) SILICON ISOTOPES OF DEEP-SEA
696 SPONGES: NEW INSIGHTS INTO BIOMINERALISATION AND SKELETAL STRUCTURE.
- 697 Cathalot, C., Van Oevelen, D., Cox, T.J., Kutti, T., Lavaleye, M., Duineveld, G. and Meysman, F.J.
698 (2015) Cold-water coral reefs and adjacent sponge grounds: Hotspots of benthic respiration and
699 organic carbon cycling in the deep sea. *Frontiers in Marine Science* 2, 37.
- 700 Chase, Z., Anderson, R.F., Fleisher, M.Q. and Kubik, P.W. (2003) Accumulation of biogenic and
701 lithogenic material in the Pacific sector of the Southern Ocean during the past 40,000 years. *Deep-*
702 *Sea Research II* 50, 799-832.
- 703 Conley, D.J., Frings, P.J., Fontorbe, G., Clymans, W., Stadmark, J., Hendry, K.R., Marron, A.O. and De
704 La Rocha, C.L. (2017) Biosilicification drives a decline of dissolved Si in the oceans through geologic
705 time. *Frontiers in Marine Science* 4, 397.
- 706 De La Rocha, C. and Bickle, M. (2005) Sensitivity of silicon isotopes to whole-ocean changes in the
707 silica cycle. *Marine Geology* 217, 267-282.
- 708 De La Rocha, C.L. (2003) Silicon isotope fractionation by marine sponges and the reconstruction of
709 the silicon isotope composition of ancient deep water. *Geology* 31, 423-426.

710 de Souza, G.F., Reynolds, B.C., Rickli, J., Frank, M., Saito, M.A., Gerringa, L.J.A. and Bourdon, B. (2012)
711 Southern Ocean control of silicon stable isotope distribution in the deep Atlantic Ocean. *Global*
712 *Biogeochemical Cycles* 26, doi:10.1029/2011GB004141.

713 DeMaster, D.J. (1979) *Marine budgets of silica and ³²Si*. Yale Univ., New Haven, CT (USA).

714 Douthitt, C.B. (1982) The geochemistry of the stable isotopes of silicon. *Geochimica et*
715 *Cosmochimica Acta* 46, 1449-1458.

716 Egan, K., Rickaby, R.E.M., Hendry, K.R. and Halliday, A.N. (2013) Opening the gateways for diatoms
717 primes Earth for Antarctic glaciation. *Earth and Planetary Science Letters*.

718 Ellwood, M.J., Kelly, M., Maher, W.A. and de Deckker, P. (2006) Germanium incorporation into
719 sponge spicules: development of a proxy for reconstructing inorganic germanium and silicon
720 concentrations in seawater. *Earth and Planetary Science Letters* 243, 749-759.

721 Ellwood, M.J., Wille, M. and Maher, W. (2010) Glacial silicic acid concentrations in the Southern
722 Ocean. *Science* 330, 1088-1091.

723 Fallon, S., James, K., Norman, R., Kelly, M. and Ellwood, M. (2010) A simple radiocarbon dating
724 method for determining the age and growth rate of deep-sea sponges. *Nuclear Instruments and*
725 *Methods in Physics Research Section B: Beam Interactions with Materials and Atoms* 268, 1241-
726 1243.

727 Fontorbe, G., Frings, P.J., Christina, L., Hendry, K.R. and Conley, D.J. (2016) A silicon depleted North
728 Atlantic since the Palaeogene: Evidence from sponge and radiolarian silicon isotopes. *Earth and*
729 *Planetary Science Letters* 453, 67-77.

730 Fontorbe, G., Frings, P.J., De La Rocha, C.L., Hendry, K.R., Carstensen, J. and Conley, D.J. (2017)
731 Enrichment of dissolved silica in the deep Equatorial Pacific during the Eocene-Oligocene.
732 *Paleoceanography*.

733 Frings, P.J., Clymans, W., Fontorbe, G., Christina, L. and Conley, D.J. (2016) The continental Si cycle
734 and its impact on the ocean Si isotope budget. *Chemical Geology* 425, 12-36.

735 Georg, R.B., Reynolds, B.C., Frank, M. and Halliday, A.N. (2006) New sample preparation techniques
736 for the determination of Si isotopic composition using MC-ICPMS. *Chemical Geology* 235, 95-104.

737 Georg, R.B., West, A.J., Basu, A.R. and Halliday, A.N. (2009) Silicon fluxes and isotope composition of
738 direct groundwater discharge into the Bay of Bengal and the effect on the global ocean silicon
739 budget. *Earth and Planetary Science Letters* 283, 67-74.

740 Goodwin, C., Berman, J., Downey, R. and Hendry, K. (2016) Carnivorous sponges (Porifera,
741 Demospongiae, Poecilosclerida, Cladorhizidae) from the Drake Passage (Southern Ocean) with a
742 description of eight new species and a review of the family Cladorhizidae in the Southern Ocean.
743 *Invertebrate Systematics*.

744 Grasse, P., Brzezinski, M.A., Cardinal, D., de Souza, G.F., Andersson, P., Closset, I., Cao, Z., Dai, M.,
745 Ehlert, C. and Estrade, N. (2017) GEOTRACES inter-calibration of the stable silicon isotope
746 composition of dissolved silicic acid in seawater. *Journal of Analytical Atomic Spectrometry* 32, 562-
747 578.

748 Guillermic, M., Lalonde, S.V., Hendry, K.R. and Rouxel, O.J.J.G.e.C.A. (2017) The isotope composition
749 of inorganic Germanium in seawater and deep sea sponges. 212, 99-118.

750 Harrison, K.G. (2000) Role of increased marine silica input on paleo-pCO₂ levels. *Paleoceanography*
751 15, 292-298.

752 Hawkings, J.R., Hatton, J.E., Hendry, K.R., de Souza, G.F., Wadham, J.L., Ivanovic, R., Kohler, T.J.,
753 Stibal, M., Beaton, A. and Lamarche-Gagnon, G. (2018) The silicon cycle impacted by past ice sheets.
754 *Nature Communications* 9, 3210.

755 Hendry, K.R. (2017) RRS Discovery Cruise DY081, July 6th – August 8th 2017. National Marine
756 Facilities.

757 Hendry, K.R. and Andersen, M.B. (2013) The zinc isotopic composition of siliceous marine sponges:
758 investigating nature's sediment traps. *Chemical Geology*.

759 Hendry, K.R. and Brzezinski, M.A. (2014) Using silicon isotopes to understand the role of the
760 Southern Ocean in modern and ancient biogeochemistry and climate *Quaternary Science Reviews*
761 89, 13-26.

762 Hendry, K.R., Georg, R.B., Rickaby, R.E.M., Robinson, L.F. and Halliday, A.N. (2010) Deep ocean
763 nutrients during the Last Glacial Maximum deduced from sponge silicon isotopic compositions. *Earth*
764 *and Planetary Science Letters* 292, 290-300.

765 Hendry, K.R., Gong, X., Knorr, G., Pike, J. and Hall, I.R. (2016) Deglacial diatom production in the
766 tropical North Atlantic driven by enhanced silicic acid supply. *Earth and Planetary Science Letters*
767 438, 122-129.

768 Hendry, K.R., Leng, M.J., Robinson, L.F., Sloane, H.J., Blusztjan, J., Rickaby, R.E.M., Georg, R.B. and
769 Halliday, A.N. (2011) Silicon isotopes in Antarctic sponges: an interlaboratory comparison. *Antarctic*
770 *Science* 23, 34-42.

771 Hendry, K.R., Marron, A.O., Vincent, F., Conley, D.J., Gehlen, M., Ibarbalz, F.M., Quéguiner, B. and
772 Bowler, C.J.F.i.M.S. (2018) Competition between silicifiers and non-silicifiers in the past and present
773 ocean and its evolutionary impacts. 5, 22.

774 Hendry, K.R. and Robinson, L.F. (2012) The relationship between silicon isotope fractionation in
775 sponges and silicic acid concentration: modern and core-top studies of biogenic opal. *Geochimica et*
776 *Cosmochimica Acta* 81, 1-12.

777 Hendry, K.R., Robinson, L.F., McManus, J.F. and Hays, J.D. (2014) Silicon isotopes indicate enhanced
778 carbon export efficiency in the North Atlantic during deglaciation. *Nature Communications* 5.

779 Hendry, K.R., Robinson, L.F., Meredith, M.P., Mulitza, S., Chiessi, C.M. and Arz, H. (2012) Abrupt
780 changes in high-latitude nutrient supply to the Atlantic during the last glacial cycle. *Geology* 40, 123-
781 126.

782 Hendry, K.R., Swann, G.E.A., Leng, M.J., Sloane, H.J., Goodwin, C., Berman, J. and Maldonado, M.
783 (2015) Technical Note: Silica stable isotopes and silicification in a carnivorous sponge *Asbestopluma*
784 *sp.* *Biogeosciences* 12, 3489-3498.

785 Hogg, M., Tendal, O., Conway, K., Pomponi, S., Van Soest, R., Gutt, J., Krautter, M. and Roberts, J.
786 (2010) Deep-seas Sponge grounds: reservoirs of biodiversity.

787 Hooper, J.N. and Van Soest, R.W. (2002) *Systema Porifera. A guide to the classification of sponges.*
788 Springer.

789 Horn, M.G., Beucher, C., Robinson, R.S. and Brzezinski, M.A. (2011) Southern Ocean nitrogen and
790 silicon dynamics during the last deglaciation. *Earth and Planetary Science Letters* 310, 334-339.

791 Howell, K.-L., Piechaud, N., Downie, A.-L. and Kenny, A. (2016) The distribution of deep-sea sponge
792 aggregations in the North Atlantic and implications for their effective spatial management. *Deep Sea*
793 *Research I: Oceanographic Research Papers* 115, 309-320.

794 Howell, K.L., Grehan, A., Piechaud, N., Ross, R., Grassie, A., English, G., NacCarthy, M. and Brereton,
795 R. (2015) Mapping The Deep: The Application Of Predictively Modelled Maps To European Spatial
796 Planning. EUROFLEETS2 Cruise Summary Report RV Celtic Explorer, Cruise No. CE15011. 50pp.

797 Hughes, H.J., Delvigne, C., Korntheuer, M., Jong, J.d., Andre, L. and Cardinal, D. (2011) Controlling the
798 mass bias introduced by anionic and organic matrices in silicon isotopic measurements by MC-ICP-
799 MS. *Journal of Analytical Atomic Spectrometry* 26, 1892-1896.

800 Hydes, D., Aoyama, M., Aminot, A., Bakker, K., Becker, S., Coverly, S., Daniel, A., Dickson, A., Grosso,
801 O. and Kerouel, R. (2010) Recommendations for the determination of nutrients in seawater to high
802 levels of precision and inter-comparability using continuous flow analysers. GO-SHIP (Unesco/IOC).

803 Jo, B.H., Kim, C.S., Jo, Y.K., Cheong, H. and Cha, H.J. (2016) Recent developments and applications of
804 bioinspired silicification. *Korean Journal of Chemical Engineering* 33, 1125-1133.

805 Jochum, K., Schuessler, J., Wang, X.H., Stoll, B., Weis, U., Müller, W., Haug, G., Andreae, M. and
806 Froelich, P. (2017) Whole-Ocean Changes in Silica and Ge/Si Ratios During the Last Deglacial
807 Deduced From Long-Lived Giant Glass Sponges. *Geophysical Research Letters* 44.

808 Kenchington, E., Beazley, L.I. and Yashayaev, I. (2016) Hudson 2016-019 International Deep Sea
809 Science Expedition Cruise Report, Canadian Data Report of Fisheries and Aquatic Sciences 1277.
810 Bedford Institute of Oceanography.

811 Kenchington, E., Power, D. and Koen-Alonso, M. (2013) Associations of demersal fish with sponge
812 grounds on the continental slopes of the northwest Atlantic. *Marine Ecology Progress Series* 477,
813 217-230.

814 Knudby, A., Kenchington, E. and Murillo, F.J. (2013) Modeling the distribution of *Geodia* sponges and
815 sponge grounds in the Northwest Atlantic. *PloS one* 8, e82306.

816 López-Acosta, M., Leynaert, A., Grall, J., Maldonado, M.J.L. and *Oceanography* (2018) Silicon
817 consumption kinetics by marine sponges: An assessment of their role at the ecosystem level.

818 López-Acosta, M., Leynaert, A., Maldonado, M.J.L. and *Oceanography* (2016) Silicon consumption in
819 two shallow-water sponges with contrasting biological features. 61, 2139-2150.

820 Maldonado, M., Aguilar, R., Bannister, R.J., Bell, J.J., Conway, K.W., Dayton, P.K., Díaz, C., Gutt, J.,
821 Kelly, M. and Kenchington, E.L. (2017) Sponge grounds as key marine habitats: a synthetic review of
822 types, structure, functional roles, and conservation concerns. *Marine Animal Forests: The Ecology of*
823 *Benthic Biodiversity Hotspots*, 145-183.

824 Maldonado, M., Navarro, L., Grasa, A., Gonzalez, A. and Vaquerizo, I. (2011) Silicon uptake by
825 sponges: a twist to understanding nutrient cycling on continental margins. *Nature Scientific Reports*
826 1, doi:10.1038/srep00030.

827 Maldonado, M., Ribes, M. and van Duyl, F.C. (2012) Nutrient fluxes through sponges: biology,
828 budgets, and ecological implications, *Advances in marine biology*. Elsevier, pp. 113-182.

829 Maldonado, M. and Riesgo, A. (2007) Intra-epithelial spicules in a homosclerophorid sponge. *Cell*
830 *Tissue Research* 328, 639-650.

831 Marron, A.O., Ratcliffe, S., Wheeler, G.L., Goldstein, R.E., King, N., Not, F., De Vargas, C. and Richter,
832 D.J. (2016) The Evolution of Silicon Transport in Eukaryotes. *Molecular Biology and Evolution* 33,
833 3226-3248.

834 Matsumoto, K. and Sarmiento, J.L. (2008) A corollary to the silicic acid leakage hypothesis.
835 *Paleoceanography* 23, doi:10.1029/2007PA001515.

836 Milligan, A.J., Varela, D.E., Brzezinski, M.A. and Morel, F.M.M. (2004) Dynamics of silicon metabolism
837 and silicon isotopic discrimination in a marine diatom as a function of pCO₂. *Limnology and*
838 *Oceanography* 49, 322-329.

839 Müller, W.E., Schröder, H.C., Burghard, Z., Pisignano, D. and Wang, X. (2013) Silicateins—a novel
840 paradigm in bioinorganic chemistry: enzymatic synthesis of inorganic polymeric silica. *Chemistry—A*
841 *European Journal* 19, 5790-5804.

842 Müller, W.E., Wang, X., Burghard, Z., Bill, J., Krasko, A., Boreiko, A., Schloßmacher, U., Schröder, H.C.
843 and Wiens, M. (2009) Bio-sintering processes in hexactinellid sponges: Fusion of bio-silica in giant
844 basal spicules from *Monorhaphis chuni*. *Journal of structural biology* 168, 548-561.

845 Müller, W.E.G., Schloßmacher, U., Wang, X., Boreiko, A., Brandt, D., Wolf, S.E., Tremel, W. and
846 Schroeder, H.C. (2007) Poly(silicate)-metabolizing silicatein in siliceous spicules and silicasomes of
847 demosponges comprises dual enzymatic activities (silica polymerase and silica esterase). *FEBS Journal*
848 275, 362-370.

849 Murillo, F.J., Muñoz, P.D., Cristobo, J., Ríos, P., González, C., Kenchington, E. and Serrano, A. (2012)
850 Deep-sea sponge grounds of the Flemish Cap, Flemish Pass and the Grand Banks of Newfoundland
851 (Northwest Atlantic Ocean): distribution and species composition. *Marine Biology Research* 8, 842-
852 854.

853 Opfergelt, S., Burton, K.W., Pogge von Strandmann, P.A.E., Gislason, S.R. and Halliday, A.N. (2013)
854 Riverine silicon isotope variations in glaciated basaltic terrains: Implications for the Si delivery to the
855 ocean over glacial-interglacial intervals. *Earth and Planetary Science Letters* 369-370, 211-219.

856 Reincke, T. and Barthel, D. (1997) Silica uptake kinetics of *Halichondria panicea* in Kiel Bight. *Marine*
857 *Biology* 129, 591-593.

858 Reynolds, B.C., Aggarwal, J., Andre, L., Baxter, D., Beucher, C., Brzezinski, M.A., Engstrom, E., Georg,
859 R.B., Land, M., Leng, M.J., Opfergelt, S., Rodushkin, I., Sloane, H.J., van der Boorn, S.H.J.M., Vroon,
860 P.Z. and Cardinal, D. (2007) An inter-laboratory comparison of Si isotope reference materials. *Journal*
861 *of Analytical Atomic Spectrometry* 22, 561-568.

862 Rice, A., Thurston, M. and New, A.J.P.i.O. (1990) Dense aggregations of a hexactinellid sponge,
863 *Pheronema carpenleri*, in the Porcupine Seabight (northeast Atlantic Ocean), and possible causes.
864 24, 179-196.

865 Riesgo, A., Maldonado, M., López-Legentil, S. and Giribet, G.J.J.o.m.e. (2015) A Proposal for the
866 Evolution of Cathepsin and Silicatein in Sponges. 80, 278-291.

867 Rousseau, J., Ellwood, M.J., Bostock, H. and Neil, H. (2016) Estimates of late Quaternary mode and
868 intermediate water silicic acid concentration in the Pacific Southern Ocean. *Earth and Planetary*
869 *Science Letters* 439, 101-108.

870 Schrader, H.J. (1972) Anlösung und Konservation von Diatomeenschalen beim Absinken am Beispiel
871 des Landsort-Tiefs in der Ostsee. *Nova Hedwigia Beih* 39.

872 Schroeder, H.C., Krasko, A., Le Pennee, G., Adell, T., Wiens, M., H., H., Müller, M. and Müller, W.E.G.
873 (2003) Silicase, an enzyme which degrades biogenous amorphous silica: contribution to the
874 metabolism of silica deposition in the demosponge *Suberites domuncula*. *Prog. Mol. Subcell. Biol.*
875 33, 249-268.

876 Shimizu, K., Cha, J., Stucky, G.D. and Morse, D.E. (1998) Silicatein a: Cathepsin L-like protein in
877 sponge biosilica. *Proceedings of the National Academy of Sciences of the USA* 95, 6234-6238.

878 Tabachnick, K., Janussen, D. and Menshenina, L. (2017) Cold biosilicification in Metazoan:
879 Psychrophilic glass sponges, *Extreme Biomimetics*. Springer, pp. 53-80.

880 Tréguer, P., Bowler, C., Moriceau, B., Dutkiewicz, S., Gehlen, M., Aumont, O., Bittner, L., Dugdale, R.,
881 Finkel, Z. and Iudicone, D. (2018) Influence of diatom diversity on the ocean biological carbon pump.
882 *Nature Geoscience* 11, 27.

883 Tréguer, P. and De la Rocha, C.L. (2013) The world ocean silica cycle. *Annual Review of Marine*
884 *Science* 5, 477-501.

885 Vacelet, J. (2006) New carnivorous sponges (Porifera, Poecilosclerida) collected from manned
886 submersibles in the deep Pacific. *Zoological Journal of the Linnean Society* 148, 553-584.

887 Vacelet, J. and Dupont, E. (2004) Prey capture and digestion in the carnivorous sponge *Asbestopluma*
888 *hypogea* (Porifera: Demospongiae). *Zoomorphology* 123, 179-190.

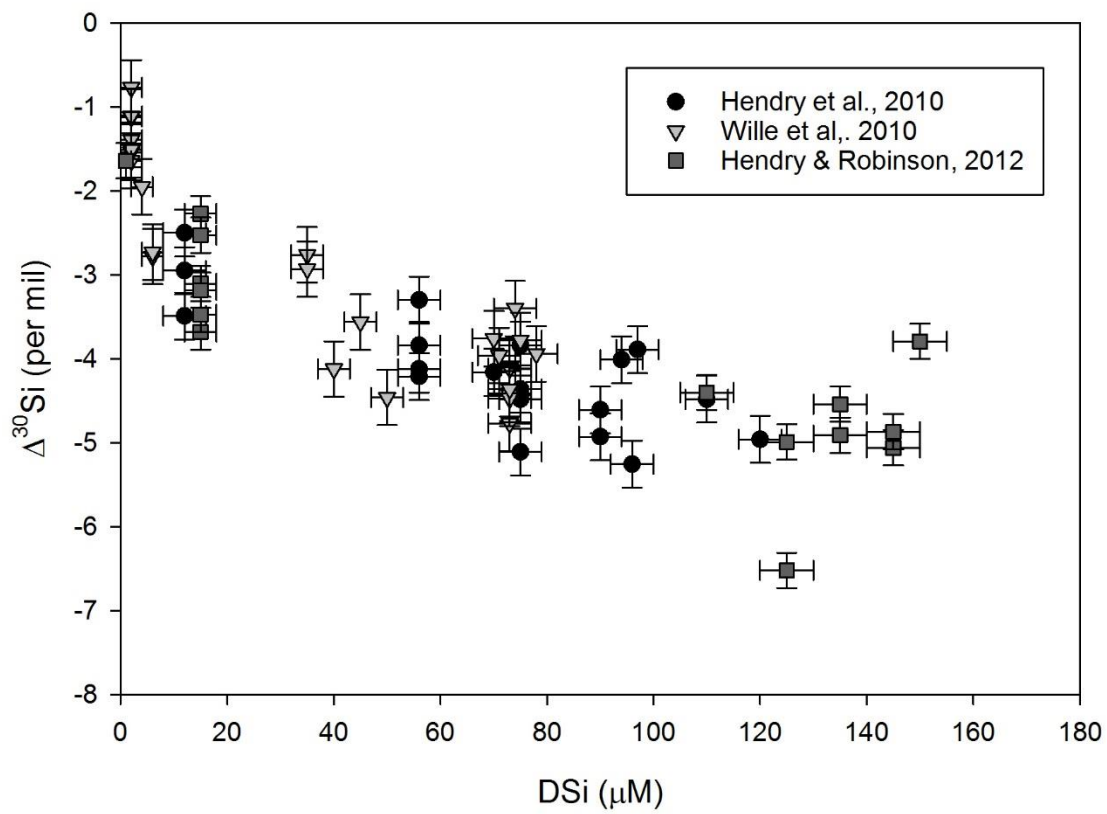
889 Wang, X., Schröder, H.C., Brandt, D., Wiens, M., Lieberwirth, I., Glasser, G., Schloßmacher, U., Wang,
890 S. and Müller, W.E.J.C. (2011) Sponge biosilica formation involves syneresis following
891 polycondensation in vivo. 12, 2316-2324.

892 Wang, X., Schröder, H.C. and Müller, W.E. (2009) Giant Siliceous Spicules From the Deep-sea Glass
893 Sponge *Monorhaphis chuni*. *International review of cell molecular Biology and Evolution* 273, 69-
894 115.

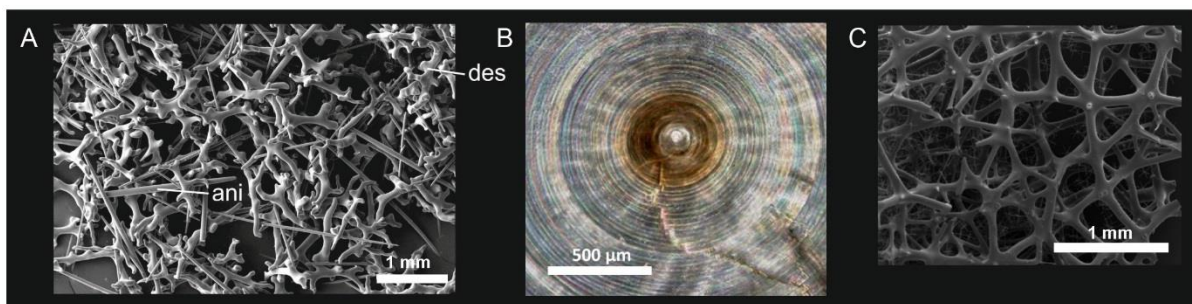
895 Weaver, J.C., Morse, D.E.J.M.r. and technique (2003) Molecular biology of demosponge axial
896 filaments and their roles in biosilicification. 62, 356-367.

897 Wille, M., Sutton, J., Ellwood, M.J., Sambridge, M., Maher, W., Eggins, S. and Kelly, M. (2010) Silicon
898 isotopic fractionation in marine sponges: a new model for understanding silicon isotopic
899 fractionation in sponges. *Earth and Planetary Science Letters*, doi:10.1016/j.epsl.2010.1001.1036.

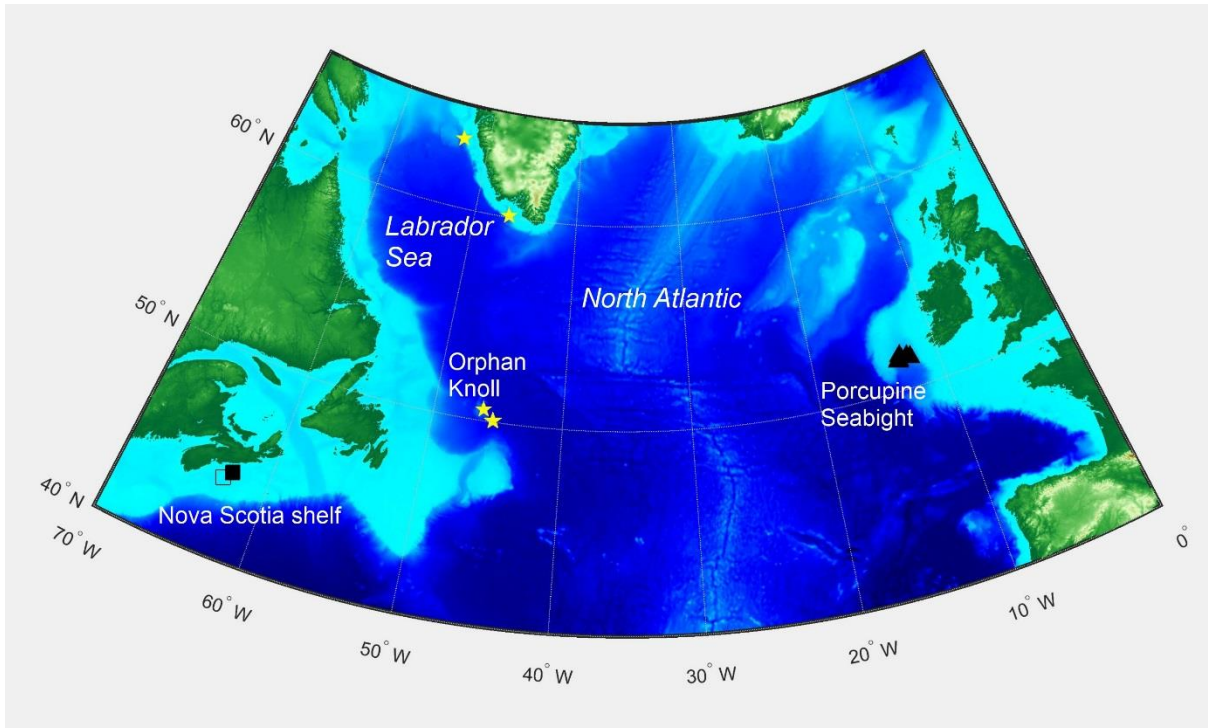
900 Woodward, E. and Rees, A. (2001) Nutrient distributions in an anticyclonic eddy in the northeast
901 Atlantic Ocean, with reference to nanomolar ammonium concentrations. *Deep Sea Research Part II:*
902 *Topical Studies in Oceanography* 48, 775-793.



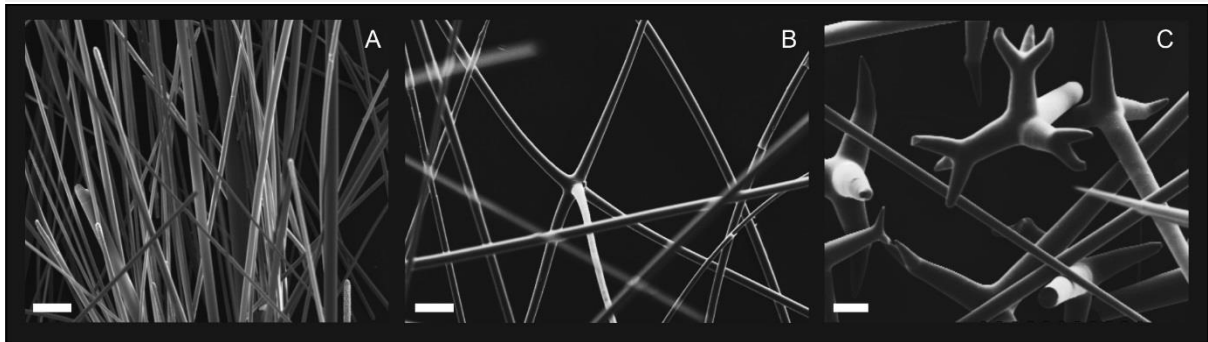
903



904



905



906

